Supporting Information

Dumbauld et al. 10.1073/pnas.1216209110

SI Methods

Cells and Reagents. Vinculin-null mouse embryonic fibroblasts (MEF1 and MEF2) were a kind gift from Eileen Adamson (Burnham Institute, La Jolla, CA). Monoclonal antibodies against vinculin (V284; Millipore) and talin (8d4; Sigma) were used for immunostaining and Western blotting. Monoclonal antibody against extracellular domain of β1 integrin (9EG7; Millipore) was used for integrin binding study. Polyclonal antibody against β1 integrin (ab1950; Chemicon) was used for adhesion blocking study. Poly(dimethylsiloxane) (PDMS) elastomers and curing agents were obtained from Dow Corning. Dithiobis(sulfosuccinimidylpropionate) (DTSSP) was purchased from Pierce Chemical. Tri(ethylene glycol)-terminated alkanethiol [$HO(CH_2CH_2O)_3$-$(CH_2)_{11}SH$] was purchased from ProChimia Surfaces. All other reagents including hexadecanethiol [$H_3C(CH_2)_{15}SH$] were purchased from Sigma. Human plasma fibronectin was purchased from Invitrogen. Vinculin head (V_H)-CFP and vinT-YFP constructs were a kind gift from Christoph Ballestrem (University of Manchester, United Kingdom).

Retroviral Vectors for Enhanced GFP-Vinculin Expression and Transduction. Retroviral plasmids pTJ66-tTA and pXF40 were previously described (1) (Fig. S1). enhanced green fluorescent protein (pEGFP)-C1 WT, T12, V_H vinculin plasmids have been described (2–5). One AgeI restriction site was inserted into the multiple cloning site of pXF40, the retroviral expression vector. The oligonucleotides 5′-AGCTTGTCAGCTACCGGTGCTACTGCA-3′ and 5′-AGCTTGCAGTAGCACCGGTAGCTGACA-3′ were annealed together, creating HindIII-compatible overhangs at each end. This product was then ligated into a linearized pXF40 vector that had been digested with HindIII. Finally, the enhanced GFP (eGFP)-vinculin constructs were digested from pEGFP-C1 with AgeI and SalI and ligated into the SalI and AgeI-digested pXF40 vector. The pXF40-eGFP-vinculin vectors transcribe the eGFP-vinculin gene from the tetracycline-inducible promoter. All vectors were verified by sequencing the ligation points.

Retroviral stocks were produced by transient transfection of helper virus-free Phoenix amphotropic producer cells with plasmid DNA (6). Vinculin-null MEFs were cultured and plated on tissue culture polystyrene at 2×10^4 cells/cm^2 24 h before retroviral transduction. Cells were transduced with 0.2 mL/cm^2 of equal parts pTJ66-tTA and pXF40-eGFP-vinculin retroviral supernatant supplemented with 4 μg/mL hexadimethrine bromide (Polybrene) and 10% FBS, and centrifuged at $1,200 \times g$ for 30 min in a swinging bucket rotor. Retroviral supernatant was replaced with growth media [DMEM, 10% (vol/vol) FBS, 100 U/mL penicillin G sodium, 100 μg/mL streptomycin sulfate, 1% nonessential amino acids, and 1% sodium pyruvate]. Five days after transduction, eGFP-expressing cells were FACS sorted, expanded, and either used for experimentation or cryopreserved. Expression of vinculin constructs was verified by Western blot and immunofluorescence microscopy.

Traction Force Measurements. Microfabricated postarray deflection device (mPAD) silicon masters were prepared as previously described (7). The elastomeric micropost arrays were fabricated using PDMS replica molding. To make a microfabricated post array template, PDMS prepolymer was cast on top of mPAD silicon masters, cured at 110 °C for 1 h, peeled off, oxidized with oxygen plasma (Plasma-Preen; Terra Universal), and silanized with (tridecafluoro-1,1,2,2,-tetrahydrooctyl)-1-trichlorosilane vapor overnight under vacuum. To make the final PDMS mPAD device, PDMS prepolymer was cast on the template, degassed under vacuum, and cured at 110 °C for 20 h and peeled off the template. Peeling-induced collapse of the mPADs was rectified by sonication in 100% ethanol, followed by supercritical drying in liquid CO_2 using a critical point dryer (Samdri-PVT-3D; Tousimis).

Flat PDMS stamps were generated by casting PDMS prepolymer on silanized silicon wafers. Stamps were coated in saturating concentration of fibronectin (FN) (50 μg/mL in PBS) for 1 h. These stamps were washed in distilled water and dried under a stream of N_2. FN-coated stamps were placed in contact with surface-oxidized mPAD substrates (UVO-Model 342; Jelight). mPAD substrates were labeled with 5 μg/mL of Δ^9-DiI (Invitrogen) in distilled water for 1 h. mPAD substrates were then transferred to a solution of 0.1% Pluronics F127 (Sigma-Aldrich) to prevent nonspecific protein absorption. WT, V_H, T12, and null eGFP-vinculin MEF cells were seeded in growth medium and then allowed to spread overnight.

mPAD substrates were transferred to an aluminum coverslip holder (Attoflour Cell Chamber; Invitrogen) for live cell microscopy and placed in a stage top incubator that regulated temperature, humidity, and CO_2 (Live Cell; Pathology Devices). Confocal images were taken with a Nikon A1-Confocal Module connected to a Nikon TE-300 inverted microscope using a high magnification objective (CFI Plan Apochromat total internal reflection fluorescence (TIRF) 60× oil, N.A. 1.45; Nikon). Post images were captured using a 590-nm laser, and vinculin images were captured using a 488-nm laser. For force measurements, the top and bottom of the posts were sequentially imaged and the deflection measured. The resulting force, F, was calculated using Euler-Bernoulli beam theory where

$$F = \delta \frac{3\pi E D^4}{64 L^3},$$

in which E, D, L, and δ are the Young's modulus, post diameter, post height, and post deflection. We analyzed >50 posts per condition.

Micropatterned Substrates. Micropatterned substrates were generated by microcontact printing of self-assembled monolayers of alkanethiols on gold (8). Arrays of CH_3-terminated alkanethiol circles were stamped on to Au-coated glass coverslips using a PDMS stamp. The remaining exposed areas were functionalized with a tri(ethylene glycol)-terminated alkanethiol. Patterned substrates were coated with FN (2.0 μg/mL) and blocked with 1% heat-denatured BSA. This process results in an array of FN-coated circular islands 15 μm in diameter spaced 75 μm apart to promote single cell attachment to each island.

Adhesion Strength Assay. Adhesion strength was measured using our spinning disk system (8–10). Micropatterned substrates with adherent cells were spun in PBS + 2 mM dextrose for 5 min at constant speed. The applied shear stress (τ) is given by the formula

$$\tau = 0.8 r \sqrt{\rho \mu \omega^3},$$

where r is the radial position from the center of the patterned coverslip, and ρ, μ, and ω are the fluid density, viscosity, and rotational speed, respectively. In some experiments the spinning buffer was supplemented with 5% dextran to increase the fluid

viscosity. After spinning, cells were fixed in 3.7% formaldehyde, permeabilized in 1% Triton X-100, stained with ethidium homodimer-1 (Invitrogen), and counted at specific radial positions using a 10× objective lens in a Nikon TE300 microscope equipped with a Ludl motorized stage, Spot-RT camera, and Image-Pro-6.3 analysis system. A total of 61 fields (80–100 cells per field before spinning) were analyzed, and cell counts were normalized to the number of cells in the center of the disk. The fraction of adherent cells (f) was then fitted to a sigmoid curve

$$f = \frac{1}{(1 + e^{[b(\tau - \tau_{50})]})},$$

where τ_{50} is the shear stress for 50% detachment, and b is the inflection slope. τ_{50} characterizes the mean adhesion strength for a population of cells.

Immunostaining for Integrin–FN Complexes and Focal Adhesions. Integrin binding was quantified via a cross-linking/extraction procedure (11, 12). After rinsing cultures three times with PBS, DTSSP (1.0 mM in cold PBS + 2 mM dextrose) was incubated for 30 min to cross-link integrins to their bound ligands. The cross-linking reaction was quenched by addition of Tris (50 mM in PBS) for 15 min. Uncross-linked cellular components were then extracted in 0.1% SDS containing 10 μg/mL leupeptin, 10 μg/mL aprotinin, and 350 μg/mL PMSF. Integrins cross-linked to their bound ligands were visualized by immunostaining with β_1 integrin-specific monoclonal antibody 9EG7. Integrin area fractions were quantified using a custom MATLAB image analysis script. Briefly, original images were first background subtracted. A threshold intensity mask was applied, and pixels above the specified intensity threshold were considered positive for integrin staining.

For staining of focal adhesion (FA) components, cells were permeabilized in CSK-stabilizing buffer [(0.5% Triton X-100: 10 mM Pipes buffer, 50 mM NaCl, 150 mM sucrose, 3mM $MgCl_2$, 0.5% (vol/vol) Triton X-100, 1 mM PMSF, 1 μg/mL leupeptin, 1 μg/mL aprotinin, and 1 μg/mL pepstatin] for 10 min, fixed in 3.7% formaldehyde for 5 min, blocked in 5% goat serum, and incubated with primary antibodies against FA components followed by AlexaFluor-labeled secondary antibodies (Invitrogen). Images were captured using a Nikon Eclipse E400 equipped with a 60× APO (1.49 N.A.) TIRF objective and Spot RT Camera/Software. Focal adhesion area fractions were quantified using a custom MATLAB image analysis script. Briefly, original images of immunostained cells were first background subtracted and then pixel intensity thresholded to determine FA area.

Fluorescence Recovery After Photobleaching. A confocal microscope head (Nikon C1) and inverted microscope (Nikon TE 300) equipped with a Coherent Sapphire solid-state 488 laser under the control of Nikon EZ-C1 software were used for FRAP experiments. Cells were seeded overnight on FN-coated mPADs. Cell-seeded mPADs were loaded into an Attofluor cell chamber (Invitrogen) and allow to equilibrate for >20 min. A 60× APO TIRF (1.49 N.A.) objective (Nikon) was used for imaging. Initial fluorescence intensity was measured using low laser power (1.5–2.5%) followed by photobleaching of a 0.85-μm-diameter circle inside FAs at 10% laser power for 1 zoomed pass (bleached circle is defined within 256 × 256 pixel box). The recovery of fluorescence was monitored every 7 s (10 s for V_H and T12) until a plateau in recovery was reached (5 prebleach and 30 post-bleach images were acquired in each series recorded). Image series were imported into MATLAB, where background subtraction and correction for incidental bleaching during image acquisition were applied to data extracted from the bleached region. Curves were fit to single exponential recovery model by assuming a reaction-dominated system and disregarding any effects of diffusion, and the characteristic recovery time ($t_{1/2}$) was calculated as previously described (2).

Transient Transfection of Vinculin Constructs. MEF1 cells were transfected using a Nucleofector II (Amaxa). For each sample, 2 million cells were resuspended in 100 μL of nucleofector solution MEF2 with 2.5 μg of plasmid DNA coding for indicated vinculin-eGFP construct. Plasmid-containing cell suspension was loaded into the Nucleofector cuvette and transfected with program T-20. Immediately after transfection, cells were transferred to a 1.5-mL centrifuge tube containing 500 μL of prewarmed RPMI 1640 (Invitrogen) and incubated for 15 min to minimize cell death. Cells were then transferred into 100-mL plates containing normal growth media (DMEM, 10% FBS, 1% sodium pyruvate, 1% penicillin-streptomycin, and 1% non-essential amino acids). Cells were sorted 72 h after transfection for eGFP expression and seeded onto micropatterned surfaces. The next day the spinning disk assay and immunostaining were performed.

Western Blotting. Cells were washed with PBS and lysed in cold radioimmunoprecipitation assay buffer [1% Triton X-100, 1% sodium deoxycholate, 0.1% SDS, 150 mM NaCl, 150 mM Tris-HCl (pH 7.2), 350 μg/mL phenylmethylsulfonyl fluoride, 10 μg/mL leupeptin, 10 μg/mL aprotinin, and 1 mM sodium orthovanadate] for 20 min. Lysates were pipette up and down ~25 times to shear the DNA and then clarified by centrifugation at 10,000 × g for 10 min. Protein concentration was then determined using a Micro BCA protein assay kit (Pierce). Equal amounts of protein (25 μg) were boiled in Laemmli sample buffer [2% SDS, 10% glycerol, 100 mM DTT, 60 mM Tris·HCl (pH 6.8), and 0.001% bromophenol blue] for 10 min and separated by SDS/PAGE. Proteins were transferred by electrophoresis onto nitrocellulose membranes and blocked with Blotto (5% nonfat dry milk, 0.02% sodium azide, and 0.2% Tween 20 in PBS without Ca^{2+}/Mg^{2+}) overnight at 4 °C. Membranes were incubated with appropriate antibodies in Blotto for 1 h at room temperature under gentle rocking. Membranes were washed in TBS-Tween [20 mM Tris·HCl (pH 7.6), 137 mM NaCl, and 0.1% Tween 20) for 30 min and incubated in near-infrared conjugated-secondary antibodies (LiCor Biosciences) for 30 min followed by 30 min washing in TBS-Tween. Membranes were imaged with a LiCor Odyssey Imager (LiCor Biosciences).

Statistical Analysis. Data are presented as mean ± SEM. Regression analyses were performed using SigmaPlot 2001 software (SPSS). ANOVA, Kruskal-Wallis nonparametric tests, and post hoc tests were performed in GraphPad Prism.

1. Gersbach CA, Le Doux JM, Guldberg RE, García AJ (2006) Inducible regulation of Runx2-stimulated osteogenesis. *Gene Ther* 13(11):873–882.
2. Cohen DM, Kutscher B, Chen H, Murphy DB, Craig SW (2006) A conformational switch in vinculin drives formation and dynamics of a talin-vinculin complex at focal adhesions. *J Biol Chem* 281(23):16006–16015.
3. Chen H, Choudhury DM, Craig SW (2006) Coincidence of actin filaments and talin is required to activate vinculin. *J Biol Chem* 281(52):40389–40398.
4. Cohen DM, Chen H, Johnson RP, Choudhury B, Craig SW (2005) Two distinct head-tail interfaces cooperate to suppress activation of vinculin by talin. *J Biol Chem* 280(17): 17109–17117.
5. Chen H, Cohen DM, Choudhury DM, Kioka N, Craig SW (2005) Spatial distribution and functional significance of activated vinculin in living cells. *J Cell Biol* 169(3):459–470.
6. Byers BA, Pavlath GK, Murphy TJ, Karsenty G, García AJ (2002) Cell-type-dependent up-regulation of in vitro mineralization after overexpression of the osteoblast-specific transcription factor Runx2/Cbfal. *J Bone Miner Res* 17(11):1931–1944.
7. Fu J, et al. (2010) Mechanical regulation of cell function with geometrically modulated elastomeric substrates. *Nat Methods* 7(9):733–736.
8. Gallant ND, Michael KE, García AJ (2005) Cell adhesion strengthening: Contributions of adhesive area, integrin binding, and focal adhesion assembly. *Mol Biol Cell* 16(9): 4329–4340.

9. García AJ, Ducheyne P, Boettiger D (1997) Quantification of cell adhesion using a spinning disc device and application to surface-reactive materials. *Biomaterials* 18(16): 1091–1098.
10. García AJ, Huber F, Boettiger D (1998) Force required to break alpha5beta1 integrin-fibronectin bonds in intact adherent cells is sensitive to integrin activation state. *J Biol Chem* 273(18):10988–10993.
11. García AJ, Vega MD, Boettiger D (1999) Modulation of cell proliferation and differentiation through substrate-dependent changes in fibronectin conformation. *Mol Biol Cell* 10(3):785–798.
12. Keselowsky BG, García AJ (2005) Quantitative methods for analysis of integrin binding and focal adhesion formation on biomaterial surfaces. *Biomaterials* 26(4): 413–418.

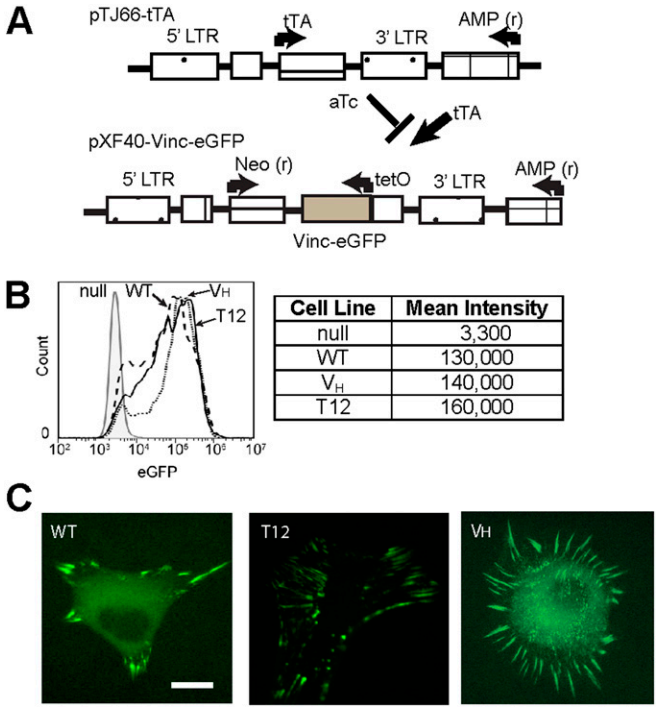

Cell Line	Mean Intensity
null	3,300
WT	130,000
V_H	140,000
T12	160,000

Fig. S1. Vinculin variant-expressing cell lines. (*A*) Maps of expression vectors. (*B*) Expression levels for vinculin variants in cell lines as determined by flow cytometry for eGFP. (*C*) Vinculin location to FAs in MEF1 cells expressing V_H and T12. (Scale bar, 10 μm.)

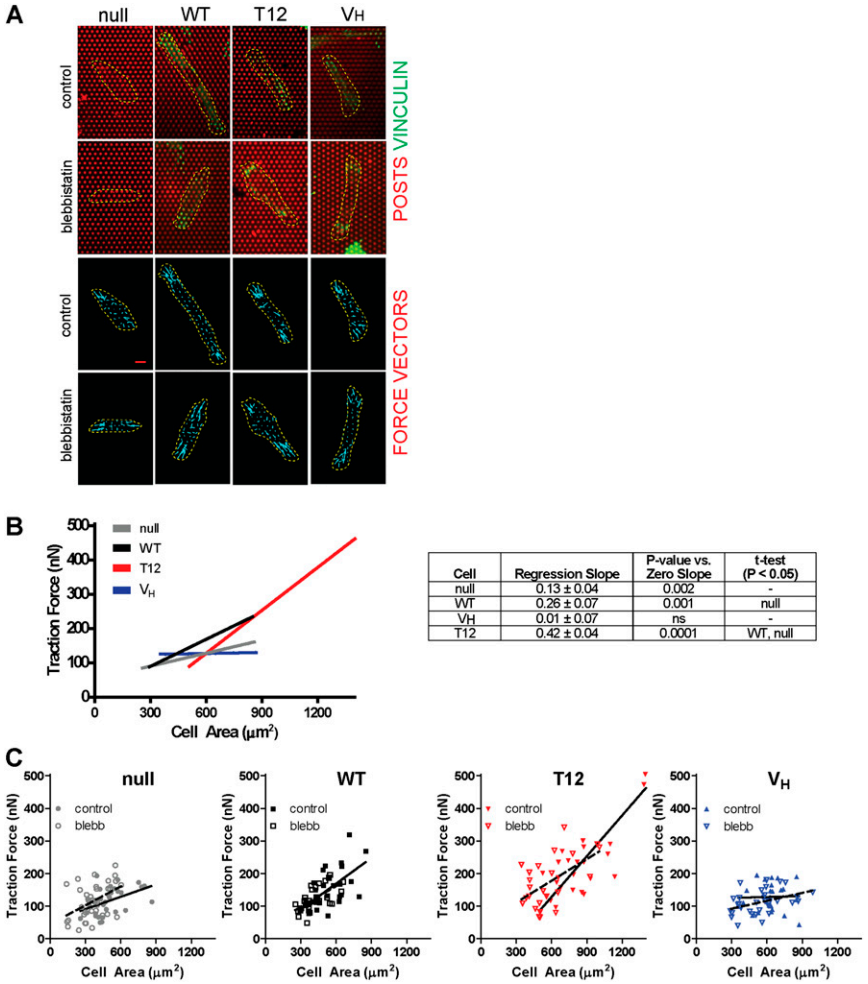

Cell	Regression Slope	P-value vs. Zero Slope	t-test (P < 0.05)
null	0.13 ± 0.04	0.002	-
WT	0.26 ± 0.07	0.001	null
VH	0.01 ± 0.07	ns	-
T12	0.42 ± 0.04	0.0001	WT, null

Fig. S2. Traction forces for vinculin-expressing cell lines in the presence or absence of blebbistatin (20 μM). (*A*) (*Upper*) Fluorescence images for FN-coated posts (red) and eGFP-vinculin (green), with cell outlined in yellow. (*Lower*) Calculated force vectors. (*B*) Linear regression fits (lines) and parameters (table, mean ± SEM) demonstrating significant differences among vinculin variants. (*C*) Plots of traction force vs. cell area for vinculin mutants, demonstrating that blebbistatin treatment does not disrupt traction force–cell area coupling. Linear fits shown as solid (control) and dashed (blebbistatin) lines.

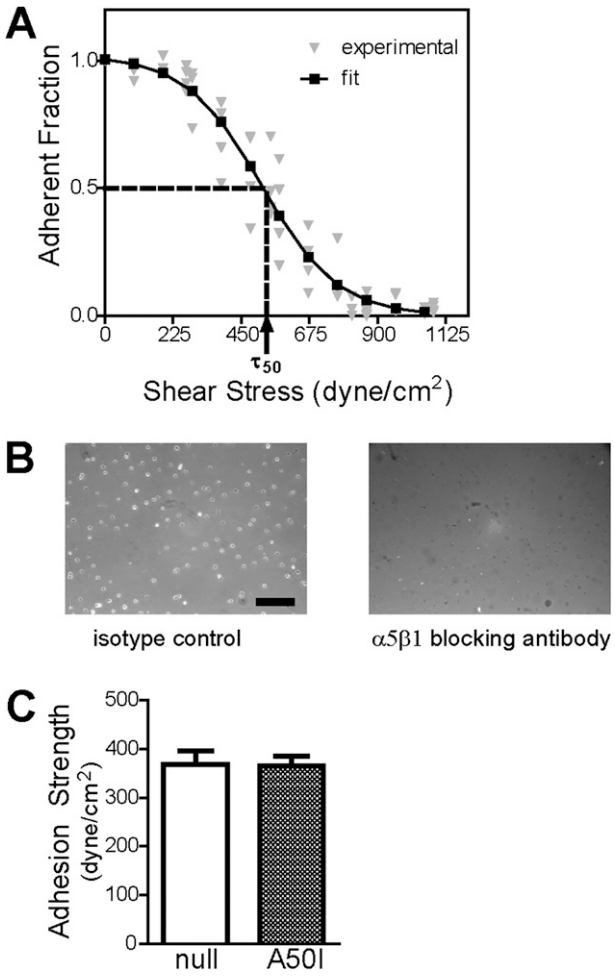

Fig. S3. Cell adhesion strength for vinculin-expressing cell lines. (*A*) Cell detachment profile showing fraction of adherent cells (f) as a function of shear stress (τ) for a single experiment. Experimental cell counts (gray triangles) are fit to a sigmoid (line, black square) to obtain the shear stress for 50% detachment (τ50), which represents the mean adhesive strength. For the experiment shown (T12), the adhesion strength is 516 dyne/cm^2 ($R^2 = 0.95$). (*B*) Adhesion of MEFs on FN coated substrates is $\alpha_5\beta_1$ integrin specific. Cells were trypsinized from dish, quenched in serum containing media, pelleted, and resuspended in appropriate antibody for 15 min with shaking. Blocking $\alpha_5\beta_1$ integrin binding to fibronectin-coated islands eliminated cell attachment to micropatterned islands compared with isotype control. (Scale bar, 200 μm.) (*C*) No differences in adhesion strength (mean ± SEM) were observed upon expression of full-length, talin-binding deficient mutant A50I.

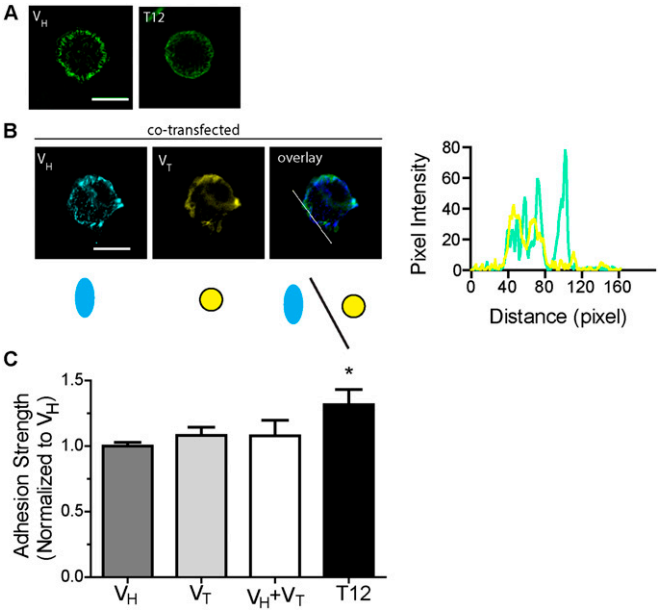

Fig. S4. Physical linkage between the head and tail domains of vinculin is required for maximal adhesion strength. (*A*) V_H and T12 constructs transiently transfected into vinculin-null cells and seeded on micropatterned islands revealed vinculin localization patterns consistent with previous results using retroviral expression of vinculin constructs. (Scale bar, 10 μm.) (*B*) Expression plasmids encoding V_H (V_H-CFP) and V_T (V_T-YFP) were cotransfected into MEF1 cells and seeded on micropatterned islands. (Scale bar, 10 μm.) Cartoon representation of the lack of physical connection between V_H and V_T. Line profile of V_H-CFP and V_T-YFP overlay demonstrates that V_T does not strongly colocalize with FA-associated V_H. (*C*) Adhesion strength (mean ± SEM) of indicated constructs transfected into vinculin-null cells. ANOVA $P < 0.02$, $^*P < 0.05$ vs. all groups.

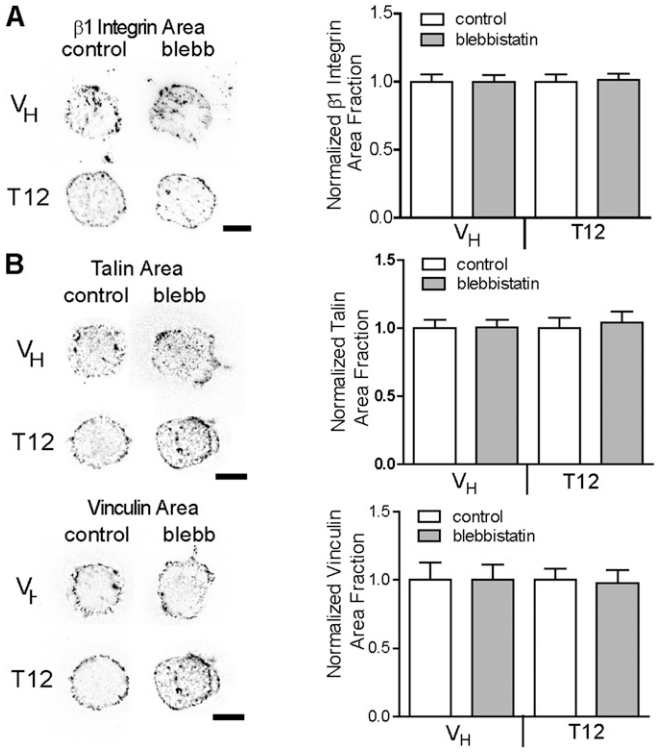

Fig. S5. Effects of blebbistatin treatment on integrin–FN complexes and focal adhesion assembly. (*A*) Immunostaining for β1 integrin in cells adhering to FN islands in the presence or absence of blebbistatin (20 μM). (Scale bar, 5 μm.) Staining is shown as grayscale on white background. Bar graph shows fraction of adhesive area occupied by integrin–FN complexes, normalized to untreated control. (*B*) Immunostaining for talin (*Upper*) and vinculin (*Lower*) in vinculin cell lines adhering to FN islands in the presence or absence of blebbistatin (20 μM). Staining is shown as grayscale on white background. Graphs present fraction of adhesive area occupied by talin and vinculin.

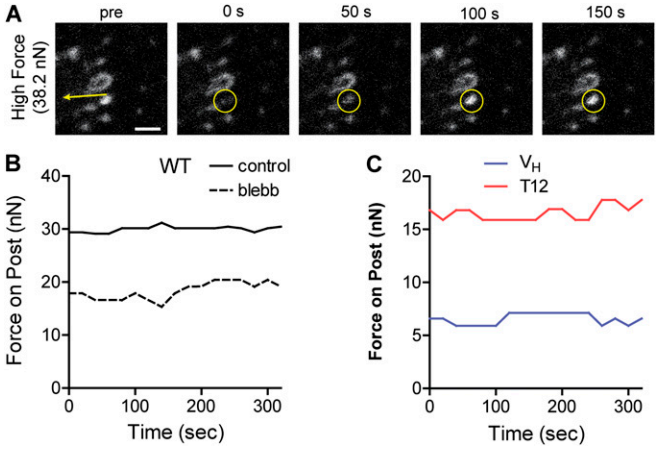

Fig. S6. Vinculin residence time at FAs depends on applied force. FRAP was performed on FAs on mPAD posts with known applied forces. (*A*) Time frames of WT-containing FA on mPADs before and after photobleaching. The yellow arrow in the prephotobleaching frame indicates the direction and magnitude of applied force, and the photobleached FA is marked with a yellow circle. (Scale bar, 4 μm.) (*B*) Force traces during FRAP experiment for WT-expressing cells in the presence and absence of blebbistatin showing constant force at FAs. (*C*) Force traces during FRAP experiment for T12- and V_H-expressing cells showing constant force at FAs.

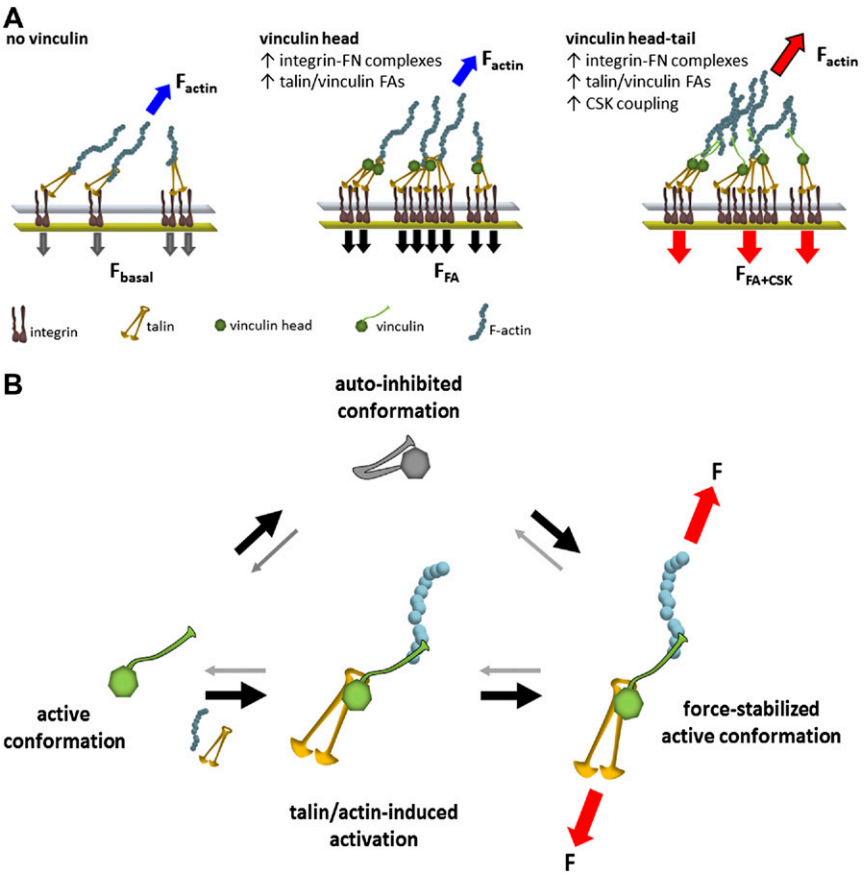

Fig. S7. Model for vinculin regulation of adhesive forces. (*A*) Vinculin differentially regulates adhesive forces. In the absence of vinculin, basal levels of adhesive forces (F_{basal}) and cytoskeletal tension (F_{actin}) are applied to integrin–ECM complexes presumably via talin. V_H increases integrin–ECM complexes and recruitment of talin and vinculin to FAs, thereby enhancing adhesive forces (F_{FA}) without influencing cytoskeletal tension. Full-length vinculin significantly enhances adhesive forces (F_{FA+CSK}) via (*i*) increasing integrin–FN complexes and talin and vinculin recruitment to FAs via V_H, and (*ii*) mechanical coupling these adhesive plaque complexes to the actin CSK. Mechanical coupling to CSK also enhances CSK tension. (*B*) Model for force-stabilized vinculin conformation. The vinculin molecule is maintained in its autoinhibited conformation via high-affinity head–tail interactions. Vinculin is activated into its open, active conformation by binding talin and actin. Force applied across the vinculin molecule stabilizes the open conformation of the molecule.

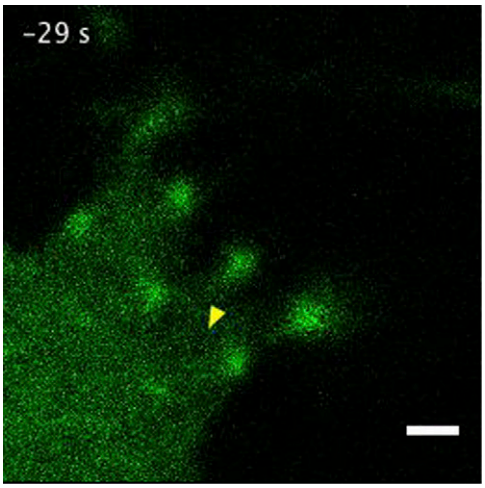

Movie S1. FRAP for WT vinculin at FAs under low applied force (FRAP-WT-3nN.avi). Movie shows fluorescence imaging of eGFP-WT expressing cells cultured on mPADs. A yellow arrow in the initial frame indicates magnitude and direction of force applied at FA (2.8 nN). A yellow circle indicates photobleached area.

Movie S1

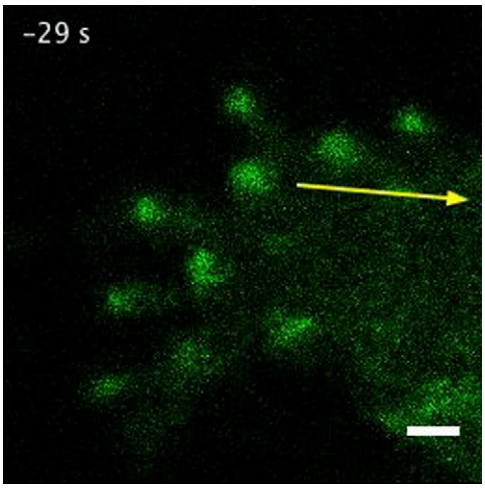

Movie S2. FRAP for WT vinculin at FAs under high applied force (FRAP-WT-29nN.avi). Movie shows fluorescence imaging of eGFP-WT expressing cells cultured on mPADs. A yellow arrow in the initial frame indicates magnitude and direction of force applied at FA (29 nN). A yellow circle indicates photobleached area.

Movie S2

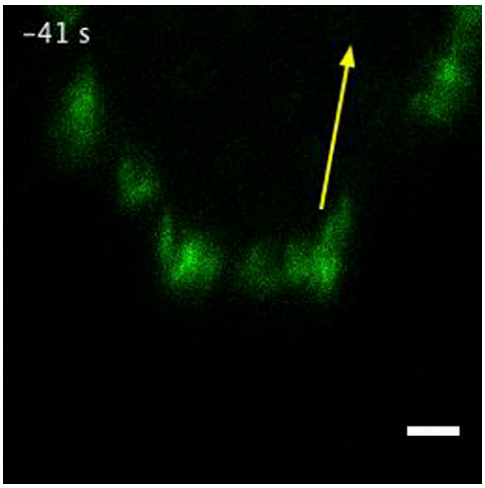

Movie S3. FRAP for T12 vinculin at FAs under high applied force (FRAP-T12-28nN.avi). Movie shows fluorescence imaging of eGFP-T12 expressing cells cultured on mPADs. A yellow arrow in the initial frame indicates magnitude and direction of force applied at FA (28.5 nN). A yellow circle indicates photobleached area.

Movie S3

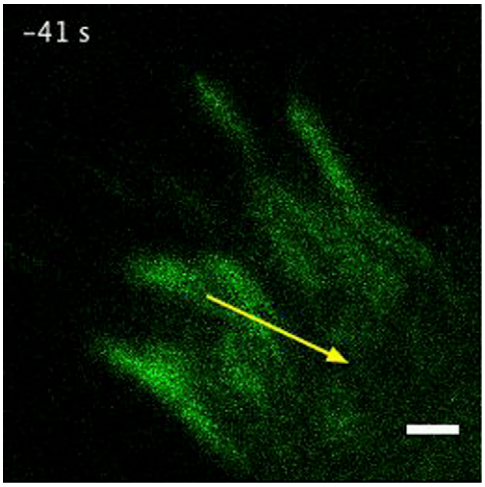

Movie S4. FRAP for V_H vinculin at FAs under high applied force (FRAP-VH-27nN.avi). Movie shows fluorescence imaging of eGFP-V_H expressing cells cultured on mPADs. A yellow arrow in the initial frame indicates magnitude and direction of force applied at FA (26.8 nN). A yellow circle indicates photobleached area.

Movie S4